RESEARCH PAPER

# Effect of the multi-sized nanoparticle distribution on the thermal conductivity of nanofluids

Sasidhar Kondaraju · E. K. Jin · J. S. Lee

**Abstract** Recent studies of nanofluids have shown that the nanoparticles when mixed in fluid medium such as water and ethylene glycol enhance the thermal conductivity of the colloids when compared to the fluid medium. However, numerous experimental studies conducted on the effective thermal conductivity of nanofluids, while using initial particle distribution consisting of range of diameters, have reported their results at volume-weighted average diameters. Here, we use computer simulations to investigate the effect of initial particle distribution or the effect of polydispersivity on the effective thermal conductivity of nanofluids. The study reveals that the simulations performed with multi-sized nanoparticles predict the effective thermal conductivity values of nanofluids closer to the experimental values than the corresponding volume weighted average diameters. Inhomogeneous coagulations in the multi-sized nanofluids were found to be a major factor for the deviation of effective thermal conductivity of the nanofluids in single- and multi-sized nanofluids. Our results suggest that initial distribution of particles has a significant role in predicting the effective thermal conductivity of nanofluids.

S. Kondaraju
Department of Aerospace and Mechanical Engineering,
University of Arizona, 1130 N. Mountain Avenue, Tucson,
AZ 85721, USA

E. K. Jin
Department of Atmospheric, Ocean and Earth Science, George
Mason University, Fairfax, VA, USA

J. S. Lee (✉)
Department of Mechanical Engineering, Yonsei University,
Seoul, Korea
e-mail: joonlee@yonsei.ac.kr

**List of symbols**

| | |
|---|---|
| $A$ | Hamaker constant |
| $C_c$ | Cunningham correction factor |
| $C_s$ | Thermal slip coefficient |
| $c_p$ | Specific heat of particle |
| $d_p$ | Diameter of particle |
| $F_B$ | Brownian force |
| $F_D$ | Hydrodynamic drag force |
| $F_p$ | Force exerted by particles on fluid |
| $F_T$ | Thermophoretic force |
| $F_V$ | Van der Waals force |
| $G_i$ | Gaussian random distribution |
| $h$ | Distance between two particles |
| $Kn$ | Knudsen number |
| $k_B$ | Boltzmann constant |
| $k_f$ | Thermal conductivity of fluid |
| $k_{nf}$ | Effective thermal conductivity of nanofluid |
| $k_r$ | Thermal conductivity ratio of particle to fluid |
| $k_T$ | Turbulent thermal conductivity |
| $m_p$ | Mass of particle |
| $Nu$ | Nusselt number |
| $N_p$ | Number of particles |
| $Pr$ | Prandtl number |
| $p$ | Pressure of fluid |
| $q_{2w}$ | Temperature coupling term |
| $Re$ | Reynolds number |
| $T_f$ | Temperature of fluid |
| $T_p$ | Temperature of particle |
| $t$ | Time |
| $u$ | Velocity of fluid |
| $v$ | Velocity of particle |
| $x$ | Position of particle |

## Greek symbols

| | |
|---|---|
| $\overline{\nabla}T$ | Mean temperature gradient |
| $\nabla t$ | Timestep |
| $\rho_{\mathrm{p}}$ | Density of particle |
| $\rho_{\mathrm{f}}$ | Density of fluid |
| $\tau_{\mathrm{T}}$ | Thermal response time of particle |
| $\tau_{\mathrm{p}}$ | Particle aerodynamic response time |
| $v$ | Kinematic viscosity of fluid |
| $\mu$ | Dynamic viscosity of fluid |
| $\delta$ | London retardation wavelength |
| $\theta$ | Fluctuation of temperature of fluid |
| $\Phi$ | Volume fraction of particles |
| $\delta(x - x^n)$ | Dirac delta function |
| $\lambda$ | Mean free path of the fluid molecule |

## Subscripts

| | |
|---|---|
| $i, j$ | Tensor directions |
| $,i$ | Differentiation w.r.t $x_i$ |
| rms | Root mean square |

## Superscripts

| | |
|---|---|
| $n$ | $n$th particle |

# 1 Introduction

Nanofluids are dilute liquid suspensions of nanoparticles with at least one of their dimensions smaller than 100 nm (Choi 1995). This new type of fluid received a lot of attention over the past decade, due to the enhanced properties and behavior associated with heat transfer activity. Researchers found an anomalous increase in the thermal conductivity, i.e., they found the thermal conductivity of nanofluids to be much larger than that predicted by classical models like Hamilton–Crosser (HC) model and Maxwell model for suspended flows, even at low volume concentrations ($\Phi$ <5%) of suspended nanoparticles (Eastman et al. 1997; Wang et al. 1999; Choi et al. 2001; Murshed et al. 2008a; Li and Peterson 2006; Zhu et al. 2006). These enhanced properties imply an enormous potential of nanofluids in industrial sectors of electronics and transportation devices.

Since thermal conductivity is most important parameter responsible for enhanced heat transfer, many experimental studies were reported on this aspect. The thermal conductivity of nanoparticles was found to vary with the size, shape and material of nanoparticles. Choi et al. (2001) found that the nanofluids with metallic nanoparticles have a higher thermal conductivity than the nanofluids with non-metallic nanoparticles. Xie et al. (2002) measured the thermal conductivity of aqueous $Al_2O_3$ with varying particle sizes and showed for the first time that the thermal conductivity of nanofluids depends strongly on particle size. Based on the experimental (Eastman et al. 1997; Wang et al. 1999; Choi

et al. 2001; Li and Peterson 2006; Xie et al. 2002) and theoretical studies (Wang et al. 1999; Eastman et al. 2004; Xuan et al. 2003; Wen and Ding 2005; Ding and Wen 2005), to explain the change in thermal conductivity of nanofluids, three main possible mechanisms were suggested: dispersion of nanoparticles, the nature of heat transport in nanoparticles, and the effects of nanoparticle clustering.

It was widely thought that the dispersion of nanoparticles alters the fluid composition and affects the energy transport process in the nanofluids; thus influencing the effective thermal conductivity of nanofluids (Wen and Ding 2005; Ding and Wen 2005). However, Beck et al. (Beck et al. 2009) studied the effect of particle size on the thermal conductivity on nanofluids for $Al_2O_3$/DIW mixture and found that the thermal conductivity of $Al_2O_3$/DIW mixture decreased with decreasing particle size. It should be noted that these results are not in agreement with previous studies; and they also contradict with the effect of Brownian motion. Mintsa et al. (2009) measured the thermal conductivity of $Al_2O_3$/DIW nanofluids for two differently sized particles at different temperatures and found that the enhancements in thermal conductivity for two different sized particles were nearly same at smaller temperatures. But at the higher temperatures, nanofluids with smaller particles showed higher enhancement. This study indicates the effect of Brownian motion on the thermal conductivity enhancement of nanofluids. Increased temperatures increase the random motion of liquid molecules, thus causing greater dispersions in the smaller sized particles. Negligible difference in the thermal conductivities of nanofluids for two differently sized particles at room temperatures can be due to the small difference among the particle sizes. Murshed et al. (2008a) and Eastman et al. (2004) showed that the interfacial interactions among the particles and liquid enhance energy transport inside the liquid and also affects heat transport in nanoparticles. Timofeeva et al. (2007), through theoretical analysis showed that the effect of interfacial interactions between particles and fluid is greater than the effect of Brownian motion. It was, experimentally by Zhu et al. (2006) and numerically by Xuan et al. (2003), shown that the clustering of nanoparticles affects the effective thermal conductivity of nanofluids negatively. Recently, researchers have also concentrated effect of pH value of liquid on the particle aggregations and the thermal conductivity enhancement of nanofluids. Wang et al. (2009) showed that the addition of dispersant to the Cu/DIW and $Al_2O_3$/DIW nanofluids increased the thermal conductivity of nanofluids. Authors related the observed phenomenon to the fact that the optimum value of pH, which is obtained by adding dispersants to nanofluids, increases the electrostatic repulsions between the particles, thus reducing the agglomeration. Zhu et al. (2009) studied the dispersion behavior of

Al₂O₃/DIW nanofluids due to the addition of sodium dodecylbenzenesulfonate (SDBS). They found that the decrease in fraction of dispersant decreases the thermal conductivity. They also found that the average particle diameter of nanoparticles was over 10 times larger in the absence of dispersant. The studies of pH value indicate that the effect of electrostatic repulsion among particles is significant with the addition of dispersant to the nanofluids. The authors have recently, using their numerical model (Kondaraju et al. 2009), shown that all the three mechanisms suggested above have a significant influence on the anomalous increase in the thermal conductivity of nanofluids.

Most of the existing experimental studies conducted on the effective thermal conductivity of nanofluids were reported for an initial single diameter (Murshed et al. 2008b). Fujimoto et al. (2001) indicated that the synthesis of nanoparticles by sonochemical reductions produce wide size distributions. Thus the authors believe that it is impracticable to create nanoparticles of single initial diameter and the thermal conductivity values reported by the experimental studies were based on the volume-weighted average diameter of the suspended particles. However, no attempt was made to study the effects of initial size distribution of particles on the final result. The authors believe that the presence of multi-sized particles in the fluid medium, due to the simultaneous influence of particles of different characteristics, change the local flow characteristics distinctly different from the single-sized particles. Cardoso and Zarrebini (2001) performed numerical simulations to study the sedimentation of poly-dispersed and mono-dispersed micro-size particles in a turbulent plume. They found that the experimental data were closer to the data obtained from the simulations of poly-dispersed particles. They suggested that the effect of the poly-dispersivity of particles on the total deposition pattern was significant, and it was over predicted by considering a root mean square particle diameter.

In this article, the authors examine the effects of the initial distribution of particles on the thermal conductivity on nanofluid. The objective of this article is to perform a nanofluid simulation: (a) using 50 differently sized particles based on the initial distribution of particles provided by Chon et al. (2005) and (b) using a volume weighted average diameter of particles provided in this paper. The authors compare the calculated effective thermal conductivity to the experimental data in Chon et al. (2005). Further to understand the effect of this multi-sized particles in nanofluids, the authors simulated nanofluids with multi-sized particles using two differently sized nanoparticles and the nanofluids using the corresponding single-sized average diameter nanoparticles.

To the authors' knowledge, a multi-sized nanofluids simulation using the Navier–Stokes method has not been carried previously. The study of the thermal conductivity of nanofluids with the suspension of multi-sized nanoparticles can give a clear understanding to the effect of initial distribution of nanoparticles. To perform above simulations, the authors used the multi-phase Navier–Stokes equations, where fluid phase was solved using the Eulerian frame and particle phase was solved using the Lagrangian frame of reference. Three possible mechanisms, dispersion of nanoparticles, the nature of heat transport in nanoparticles, and the effects of nanoparticle clustering, responsible for the anomalous increase in the thermal conductivity of nanofluids, were modeled as different terms in the nanoparticle momentum and temperature equations. Dispersion of nanoparticles was included by applying forces such as the Brownian force, thermophoresis force and van der Waals force in the nanoparticle momentum equation. The coagulation of nanoparticles was also controlled by the van der Waals force acting on the adjacent nanoparticles. Interfacial interaction between the particles and liquid was modeled by an addition of a temperature source term to the fluid temperature equation. The model was validated against the experimental values of Cu(100 nm)/DIW and Al₂O₃(80 nm)/DIW nanofluids and was observed to predict the effective thermal conductivity accurately.

The authors have previously used this model to study the thermal conductivity of nanofluids and the turbulent characteristics of nanofluids (Kondaraju et al. 2009). In this study, the authors extended the model to take into account for the suspension of multi-sized particles in the fluid medium. Details of mathematical and numerical models are provided in the next section followed by the discussion of the present results.

## 2 Mathematical model

In the Lagrangian frame of reference, the equation of motion of nanoparticle and time-dependent particle temperature equation are given by,

$$(\mathrm{d}x_i^n)/\mathrm{d}t \equiv v_i^n \tag{1}$$

$$\frac{\mathrm{d}v_i}{\mathrm{d}t} = F_{\mathrm{D}i} + F_{\mathrm{B}i} + F_{\mathrm{T}i} + F_{\mathrm{V}i} \tag{2}$$

$$\frac{\mathrm{d}T_{\mathrm{p}}}{\mathrm{d}t} = \frac{Nu}{\tau_{\mathrm{T}}} \frac{(T_{\mathrm{f}} - T_{\mathrm{p}})}{2} \tag{3}$$

where $x_i^n$ and $v_i^n$ are the instantaneous particle position and velocity of the $n$th particle, respectively. Subscript $i$ represents the tensor notation. $\tau_T$ is thermal response time of the particle and given as $\tau_{\mathrm{T}} = \frac{\rho_{\mathrm{p}} c_{\mathrm{p}} d_{\mathrm{p}}^2}{12 k_{\mathrm{f}}}$. $k_{\mathrm{f}}$, $d_{\mathrm{p}}$, $c_{\mathrm{p}}$, and $\rho_{\mathrm{p}}$ are the nanoparticle thermal conductivity of the base fluid, diameter, specific heat, and density of the particle, respectively. $Nu$ is the Nusselt number. $T_{\mathrm{f}}$ is the fluid

temperature in the neighborhood particle and $T_p$ is the temperature of the particle.

$F_{Di}$ is the hydrodynamic drag force from the fluid, which is calculated by applying the Stokes law (Maxey and Riley 1983)

$$F_{Di} = \frac{1}{\tau_p}\left(u_i(x_i^n) - v_i^n\right) \tag{4}$$

$$\tau_p = \frac{\rho_p d_p^2}{18 v \rho_f} \tag{5}$$

$\tau_p$ is the particle aerodynamic response time. $u$ is the fluid velocity in the neighborhood of the particle, $\rho_f$ is the fluid density, and $v$ is the kinematic viscosity of fluid. The Brownian force $F_{Bi}$ (Li and Ahmadi 1992) is given as in Eq. 6.

$$F_{Bi} = G_i \left(\frac{216}{\pi} \frac{v k_B T}{\rho_f d_p^5 \left(\frac{\rho_p}{\rho_f}\right)^2 C_c \Delta t}\right)^{1/2} \tag{6}$$

$G_i$ is the Gaussian random number with zero mean and unit variance. $C_c$ is known as the Cunningham correction factor. $k_B$ is the Boltzmann constant and $T$ is the initial fluid temperature. $k_B T$ is known as the thermal energy at room temperature ($=0.4 \times 10^{-20}$ J).

The contribution of thermophoretic effect (Talbot et al. 1980) $F_{Ti}$ in Eq. 7 can be given by

$$F_T = -\frac{6\pi d_p v^2 C_s (k_r + 2.18 Kn)}{\rho(1 + 3 \times 1.14 k_r)(1 + 2k_r + 4.36 Kn)} \frac{1}{m_p T} \frac{\partial T_f}{\partial x_i} \tag{7}$$

Here $k_r$ is the thermal conductivity ratio of nanoparticle to base fluid. $Kn$ is the Knudsen number defined as $Kn = \frac{2\lambda}{d_p}$ where $\lambda$ is the mean free path of the fluid molecule. $C_s$ ($=1.147$) is the thermal slip coefficient and $\frac{\partial T_f}{\partial x_i}$ is the temperature gradient of fluid in the $x_i$ direction. $m_p$ is the mass of the nanoparticle.

The van der Waals force, $F_{vi}$ is approximated as Casimir effect (Apostulou and Hrymak 2008) and is given as

$$F_{vi} = \frac{A d_{p1} d_{p2}}{12 (d_{p1} + d_{p2}) h_i^2} \delta \tag{8}$$

where $d_{p1}$ and $d_{p2}$ are diameters of two individual nanoparticles with a distance $h$ between them. $A$ is called as Hamaker constant and is of order of $10^{-19}$ J (Apostulou and Hrymak 2008). $\delta$ is called the London retardation wavelength and is set to 100 nm. As particles come in contact, Eq. 8 predicts that the colloidal force is infinite because $h$ reduces to zero. In order to prevent singularity as $h$ reduces to zero in the solution, a cut-off distance of 0.2 nm was implemented in the calculations based on the relative magnitudes of all the forces acting on the particles. When

particles are closer than this cut-off distance, particles are allowed to coagulate and a new diameter is calculated based on the sum of two coagulated particle diameters.

Time-dependent, three-dimensional Navier–Stokes equations are solved in a cubical domain with the periodic boundary condition. The non-dimensional equations for fluid can be expressed as

$$\frac{\partial u_i}{\partial t} + u_j u_{i,j} = -p_{,i} + \frac{1}{Re} u_{i,jj} - F_{pi} \tag{9}$$

$$u_{i,i} = 0 \tag{10}$$

$$\frac{\partial T_f}{\partial t} + u_j \frac{\partial T_f}{\partial x_i} = -\frac{1}{Re\,Pr} \frac{\partial^2 T_f}{\partial x_j^2} + u_2 \bar{\nabla} T + q_{2w} \tag{11}$$

where $u$ is the fluid velocity, $p$ is pressure field, $T_f$ is the fluid temperature, $Re$ is the Reynolds number, and $Pr$ is the Prandtl number. $\bar{\nabla}T$ denotes the mean temperature gradient in the $x_2$ direction, which effectively acts as a source term for the fluid temperature field. The non-dimensional value of $\bar{\nabla}T$ is taken as 1.0 in the present simulations. Subscripts $i$ and $j$ represent tensor notations; and subscripts ',i' and ',j' represent differentiation with respect to $x_i$ and $x_j$, respectively. $F_{pi}$ is the net force exerted by the particles on fluid and is shown in Eq. 12 (Sundaram and Collins 1999). $N_p$ is the total number of particles in the computational domain. $\delta(x - x^n)$ is the Dirac delta function. $v^n$ is the velocity of $n$th particle and $u(x^n)$ is the velocity of fluid at the position of the $n$th particle.

$$F_{pi} = \frac{1}{\rho_f} \sum_{n=1}^{N_p} \frac{m_p(u(x^n) - v^n)}{\tau_p} \delta(x - x^n) \tag{12}$$

As indicated in the introduction, the authors use a temperature coupling term, $q_{2w}$, to couple particle temperature source to the fluid temperature equation. This term, similar to momentum coupling term, is introduced into the model as a point source. The source term $q_{2w}$ arises because of the convective heat transfer to and from the particle. The coupling term is calculated by applying the action-reaction principle to a generic volume of fluid (here considered as grid cell) containing a particle. $q_{2w}$ is given by Eq. 13. $T_p^n$ is the temperature of $n$th particle and $T_f(x^n)$ is the fluid temperature at the position of $n$th particle. Values of $u(x^n)$ and $T_f(x^n)$ at the position of $n$th particle are obtained by interpolation.

$$q_{2w} = \sum_{n=1}^{N_p} Nu\left(T_f(x^n) - T_p^n\right)\delta(x - x^n) \tag{13}$$

To implement the multi-sized particle suspensions, the authors considered a discrete distribution of particle sizes, with a particle volume fraction of $\phi_{vk}$ with particle aerodynamic response time $\tau_{pk}$ for $k = 1, ..., n$. Here $n$ is the total number of clouds with particles of one size being

represented as one cloud. The number of particles of cloud $k$ in the suspension was determined by $N_{pk} = \phi_{vk}\frac{v_f}{v_{pk}}$, where $v_f$ is the volume of fluid and $v_{pk}$ is the volume of an individual particle of cloud $k$. The position of all $N_p$ particles was determined using the Gaussian random distribution. Particles of cloud $k$ were then assigned a velocity ($v$), temperature ($T_p$), particle aerodynamic response time ($\tau_{pk}$) and particle temperature response time ($\tau_{Tk}$). The initial temperature of particle in this simulation, irrespective of the cloud, was taken as a constant and the velocity of particles, irrespective of cloud, was initially set to zero. Initial distribution of particles for a 50 cloud nanofluid simulation is shown in Fig. 1. Differently sized particles are represented by different shades of grayscale with light shade representing the smallest particle size and dark shade representing the largest particle size.

Isotropic domain with periodic boundary conditions was used for the simulations. Fluid was initially considered to be still with particles homogeneously suspended in the domain. A $128^3$ grid size was used and the governing partial differential equations were approximated with a semi-discrete Fourier--Galerkin spectral method, employing exact dealiasing via the 3/2 rule (Canuto et al. 1987). The resulting partial differential equations were advanced in time using the low-storage, third-order Runge–Kutta scheme described by Spalart et al. (1991). The method advanced linear terms implicitly and nonlinear and inhomogeneous terms explicitly.

To study the effects of multi-sized particles, two different sections of simulations were carried out and both sections
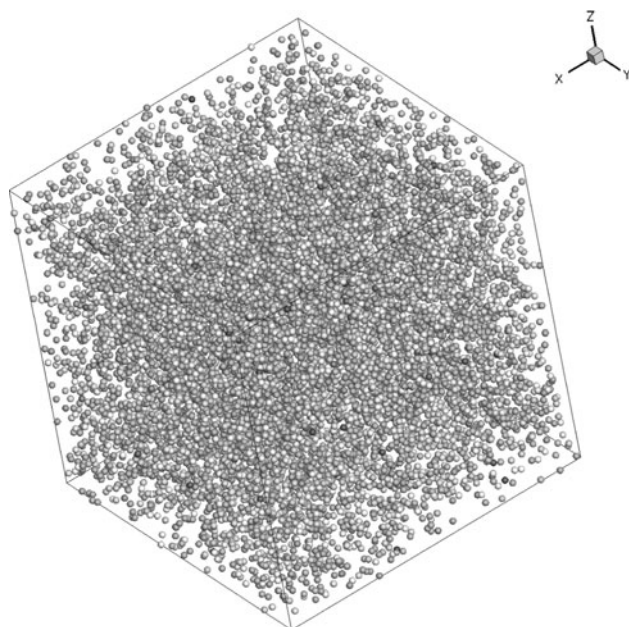
with detailed conditions were tabulated in their respective results sections. In Sect. 3.2 of results, a multi-sized particle and a single-sized particle were simulated for $Al_2O_3$/DIW nanofluids and compared with the experimental data. In order to simulate the multi-sized nanofluids case, 50 different sized particles ranging from 100–300 nm were considered. For the single-sized nanofluid case, particles with initial diameters of 182.4 nm were considered.

Further study on the effect of multi-sized particles was carried out by using Cu/DIW nanofluids with differently sized particles. Details are tabulated in Sect. 3.3 of results. Multi-sized nanofluids were simulated by mixing two differently sized nanoparticles each with 0.5% of volume fraction. The corresponding single-sized nanofluids were simulated by using an average diameter of the multi-sized nanofluids case with 1% volume fraction.

Simulations were performed using dual core AMD workstations (3 GHz CPU, 2 GB RAM processor chip) located at the Wayne State University Multi-scale Fluid Dynamics Laboratory. The simulations were terminated after 300 time steps. Non-dimensional time step of $9 \times 10^{-4}$ was used for the time integration. All cases were run until the $u_{rms}^2$ values of the fluid reached the stabilized state. Figure 2 shows the plot of $u_{rms}^2$ along the $y$-axis and time along the $x$-axis. As indicated in the plot, data were collected at $t = 0.2416$.

# 3 Results

## 3.1 Validation

To validate the model, the authors performed the simulations using the Cu(100 nm)/DIW and $Al_2O_3$(80 nm)/DIW



Fig. 1 Initial particle distribution of a simulation of nanofluid with 50 multi-sized particles is shown
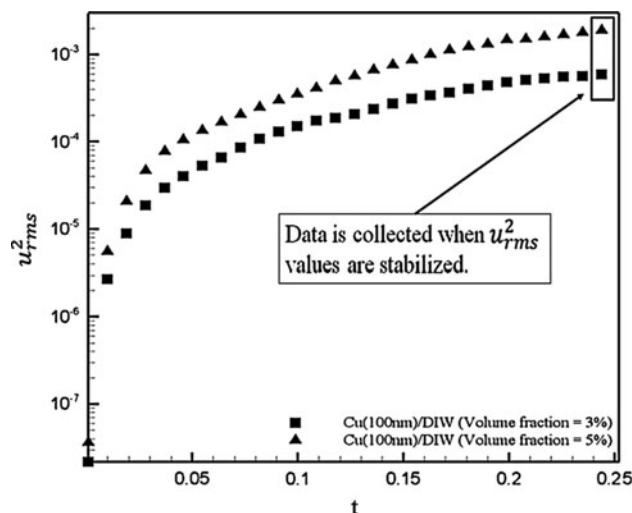


Fig. 2 RMS square velocity values were plotted against time. All data were collected when $u_{rms}^2$ were observed to be stabilized

nanofluids. The cases used for the validation are shown in Table 1. The turbulent thermal conductivity ($k_T$) was determined by the equation (Elperin et al. 1996) $\langle u(x)\theta(x)\rangle = -k_T \overline{\nabla} T$, where $\theta$ is the fluctuations of temperature. The effective thermal conductivity of nanofluid was calculated as $k_{nf}/k_f = (k_T + k_f)/k_f$, where $k_f$ is the thermal conductivity of the fluid. As expected, the effective thermal conductivity of nanofluids increases with the increase of volume fraction (Fig. 3). The numerical data of present simulations were compared with the experimental data obtained by Xuan and Li (2000) and Murshed et al. (2006). The calculated effective thermal conductivity values are observed to be in good agreement with the experimental data as shown in Fig. 3. The simulations underpredicted the effective thermal conductivity at 2% volume fraction for Cu(100 nm)/DIW nanofluid. A possible reason for this under-prediction can be the discrepancy in prediction of the coagulation of particles in the present simulations, compared to the experiments. The values of effective thermal conductivity for the 3 and 5% volume fraction cases in the present simulations were closer to the experimental values. Details about the coagulation effects will be discussed later in this article. The values of

**Table 1** The simulated cases, used for the validation of numerical model, differ on the basis of the type of nanofluid and particle sizes

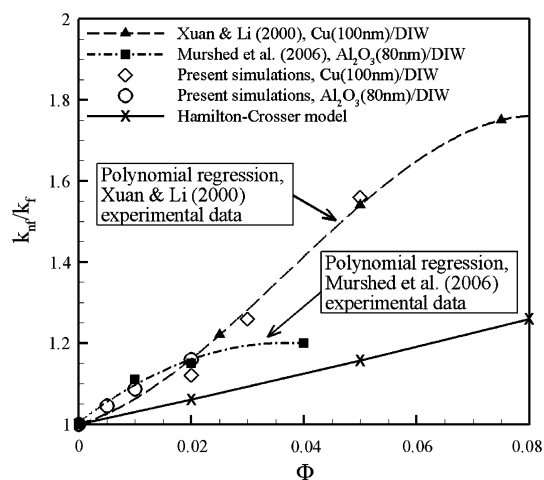| Nanofluids | Particle size (nm) | Volume fraction (%) |
|---|---|---|
| Cu/DIW | 100 | 2, 3, 5 |
| Al$_2$O$_3$/DIW | 80 | 0.5, 1, 2 |



**Fig. 3** The effective thermal conductivity values were plotted at different volume fractions for the present DNS, the experimental data and the Hamilton–Crosser model. The effective thermal conductivity values were observed to increase with the increase in volume fraction. The values calculated in current model were close to the measured experimental data. Reproduced with permission from Int J Heat Mass Trans 53 (2010). Copyright 2009 Elsevier Ltd

Hamilton–Crosser model are also included in Fig. 3. The values of the effective thermal conductivity of nanofluids predicted by the Hamilton–Crosser model were much lower than that of the present simulations and the experimental values. This is because the model does not include the effects of particle size and various forces predominantly acting on nanoparticles (Brownian force, thermophoresis force, van der Waals force) which are considered as important mechanisms for enhancing the thermal conductivity of nanofluids (Keblinski et al. 2002).

## 3.2 Comparison of a multi-sized case with experimental data

The authors have been circumspective of the use of single-sized nanoparticles in the numerical models as it is impracticable for the experimentalists to create single-sized particles for their studies. Thus the authors, in order to achieve a case in close match to a realistic case, simulated nanofluid with multi-sized particles and compared it with the experimental data of Chon et al. (Chon et al. 2005). The authors simulated an initial particle distribution profile as was used by Chon et al. (2005) in their experiments. To obtain an accurate profile, the authors used 50 differently sized particles with the volume percent of each individual particle as indicated in Chon et al. (2005). The range of particle sizes considered in the simulations was from 100 to 300 nm. The details of simulations performed in this section were shown in Table 2.

The initial distribution of particles in experiments and current simulations are shown in Fig. 4. The figure indicates a close match of the profiles shown in the experiment and the current simulations. The simulations were run until the fluid was stabilized and the effective thermal conductivity value for the multi-sized mixture case was calculated. The authors also simulated a single-sized nanofluid case for the similar conditions with a particle diameter of 182.4 nm. The diameter for the single-sized case used in the simulation was the volume weighted average diameter obtained by Chon et al. (2005), from transmission electron microscopy (TEM) images.

The effective thermal conductivity values for the multi-sized and single-sized cases are shown in Table 3. The percentage difference between the simulated value and the

**Table 2** The simulated cases, used for the comparison of multi-sized and single-sized cases with the experimental data, differ on the basis of the type of nanofluid and particle sizes

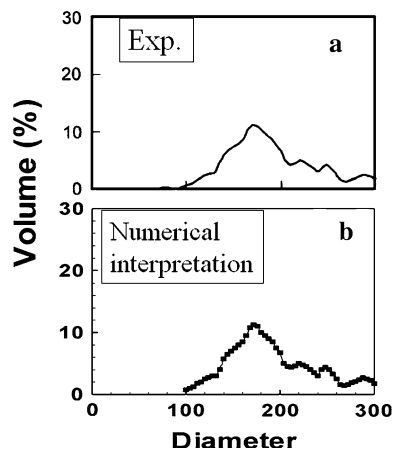| Nanofluids | Particle size (nm) | Volume fraction (%) |
|---|---|---|
| Al$_2$O$_3$/DIW (50 discrete clouds | 100–300 | 1 |
| Al$_2$O$_3$/DIW (Single cloud) | 182.4 | 1 |

Fig. 4 Initial particle distribution profile (**a**) used by (Chon et al. 2005) and **b** the profile used by the authors for the current simulations

**Table 3** The effective thermal conductivity and the percentage difference from the experimental value for multi-cloud and single cloud case

| Nanofluid | Effective thermal conductivity $(k_{nf}/k_f)$ | Percentage difference from exp. value $((k_{nf} - k_{exp})/k_{exp}) \times 100$ |
|---|---|---|
| Al$_2$O$_3$/DIW (50 discrete clouds [100–300 nm]) | 1.10117 | $8.25 \times 10^{-2}$ |
| Al$_2$O$_3$/DIW (single cloud 182.4 nm) | 1.00560 | $6.814 \times 10^{-1}$ |

experimental value was calculated for each case and also shown in Table 3. It is evident that the multi-sized particle case showed better prediction to the experimental value as compared to the single-sized case. The difference between the experimental case and the multi-sized case was as low as $8.25 \times 10^{-2}$%. The study reveals that the experimental

values of the effective thermal conductivity are affected by the presence of multi-sized particles and thus it is necessary to consider the range of initial size distribution of nanoparticles in the numerical models, when being compared with the experimental studies.

### 3.3 Effect of multi-sized particles

As discussed in Sect. 1, both two-way temperature coupling and forces acting on the particles are responsible for increasing the thermal conductivity of nanofluids, which are in turn directly dependent on the size of nanoparticle. The authors illustrate this effect in Fig. 5, where the fluid temperature field was correlated with the particle velocities and the particle temperature response time at the end of the simulation for Cu(75 nm)/DIW nanofluids. Particle positions were extracted from the slice corresponding to the fluid temperature. Figure 5a illustrates the velocities of the individual particles, with circular region representing corresponding to larger velocity and square block corresponding to the smaller velocity. It is evident that the region consisting of particles predominantly with larger velocities induces higher heat transfer in the fluid, thus decreasing the fluid temperatures. A simple explanation for this high heat transfer in the region of larger particle velocities is that the large particle velocities intensify the perturbations in the fluid medium, thus enhancing the swirling and fluctuations of fluid. The increased fluctuations in the fluid medium cause higher heat transfer rates in fluid.

From Eq. 13, it is clear that the magnitude of $q_{2w}$ is larger for smaller values of particle temperature response time ($\tau_T$). Increasing in the value of $q_{2w}$, which acts as dissipative term in the fluid temperature equation, decreases the temperature of fluid. Thus, it can be deduced that the smaller values of $\tau_T$ are responsible for higher heat
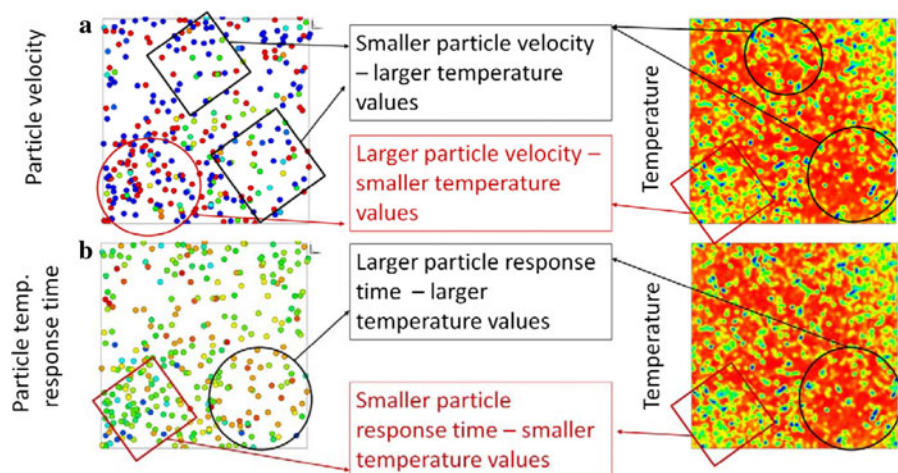


**Fig. 5** Fluid temperature in correlation with the particle velocities and particle temperature response time

**Table 4** The simulated cases, used to study the effect of multi-sized and single-sized on the effective thermal conductivity of nanofluids, differ on the basis of the type of nanofluid and particle sizes

| Nanofluids | Particle size (nm) | Volume fraction (%) |
|---|---|---|
| Cu/DIW | 63.5 | 1 |
| Cu/DIW | 50 + 75 | 0.5 + 0.5 |
| Cu/DIW | 75 | 1 |
| Cu/DIW | 50 + 100 | 0.5 + 0.5 |
| Cu/DIW | 87.5 | 1 |
| Cu/DIW | 75 + 100 | 0.5 + 0.5 |

transfer rates in fluid. A similar inference can be made from left side image of Fig. 5b, which illustrates the $\tau_T$ of the individual particles. Circular marked region, in the left side image of Fig. 5b, corresponds to largest $\tau_T$ and square region represents the smallest $\tau_T$. The region consisting of particles predominantly with smaller $\tau_T$ values show smaller fluid temperatures and the region consisting of particles predominantly with larger $\tau_T$ values show larger fluid temperatures. Figure 5 thus illustrates that both dispersion of particles and heat transport in nanoparticles have contributions in enhancing the effective thermal conductivity of nanofluids.

As explained, it is clear that the effective thermal conductivity of nanofluids is affected by the presence of differently sized particles in the fluid. To study the effect of multi-sized nanoparticles on the heat transfer in nanofluids, the authors simulated multi-sized cases and the corresponding average single-sized cases as shown in Table 4. Two distinctly sized particles were used to simulate the nanofluids with multi-sized nanoparticles suspended inside. Volume-fraction percent of each size was 0.5. The nanofluids with single-sized nanoparticles suspended inside were simulated by considering volume weighted average sized particles.

The values of the effective thermal conductivity were plotted for all cases (Fig. 6). The simulated results revealed an increase in the effective thermal conductivity for the nanofluids with multi-sized nanoparticles when compared to that of the nanofluids with the corresponding single-sized nanoparticles. It can also be observed that the between the effective thermal conductivity of multi-sized case to the corresponding single-sized case was larger when the size difference in the initially distributed particles was larger (Cu(50 + 100 nm)/DIW and Cu(75 nm)/DIW show larger difference in the effective thermal conductivity values when compared to other cases). This observation suggests a greater deviation of the effective thermal conductivity of mixture case from the single-sized case when the size difference in the initially distributed particles is larger.

Figure 6 also reveals that the Cu(50 + 75 nm)/DIW and Cu(63.5 nm)/DIW show greater deviation in the effective
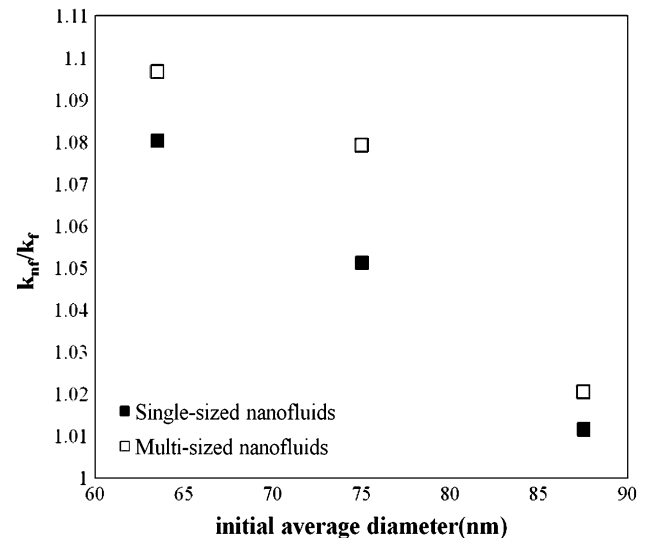


**Fig. 6** The effective thermal conductivity of multi-sized and the corresponding single-sized nanofluids. The plot shows larger effective thermal conductivities of mixture cases

**Table 5** The effective thermal conductivity and the percentage difference between the multi-sized and corresponding single-sized case

| Nanofluid | Effective thermal conductivity ($k_{nf}/k_f$) | Percentage difference |
|---|---|---|
| Cu(50 + 75 nm)/DIW | 1.096615 | 1.5168 |
| Cu(63.5 nm)/DIW | 1.08023 | |
| Cu(50 + 100 nm)/DIW | 1.07219 | 2.6600 |
| Cu(75 nm)/DIW | 1.051186 | |
| Cu(75 + 100 nm)/DIW | 1.0205 | $8.9873 \times 10^{-1}$ |
| Cu(87.5 nm)/DIW | 1.01143 | |

thermal conductivity values when compared to that of Cu(75 + 100 nm)/DIW and Cu(87.5 nm)/DIW, despite the size difference between the particles (50 + 75 nm = 25 and 75 + 100 nm = 25) in both the multi-sized cases being same. The percentage difference in the effective thermal conductivities of mixture and the corresponding single-sized cases are shown in Table 5. The percentage difference between Cu(50 + 75 nm)/DIW and Cu(63.5 nm)/DIW is 1.5168%, which is greater than the percentage difference of $8.9873 \times 10^{-1}$% between Cu(75 + 100 nm)/DIW and Cu(87.5 nm)/DIW. It suggests a possible increase in the deviation of the effective thermal conductivity between the multi-sized and the corresponding single-sized cases as the size of the particles decreases.

To understand the effect of multi-sized particles, average velocity of particles and the average $q_{2w}$ are plotted in Figs. 7 and 8, respectively. Both Figs. 7 and 8 show larger magnitudes for the multi-sized cases when compared to that of the corresponding single-sized cases. Further, it can also be observed that the deviation in the magnitudes of the
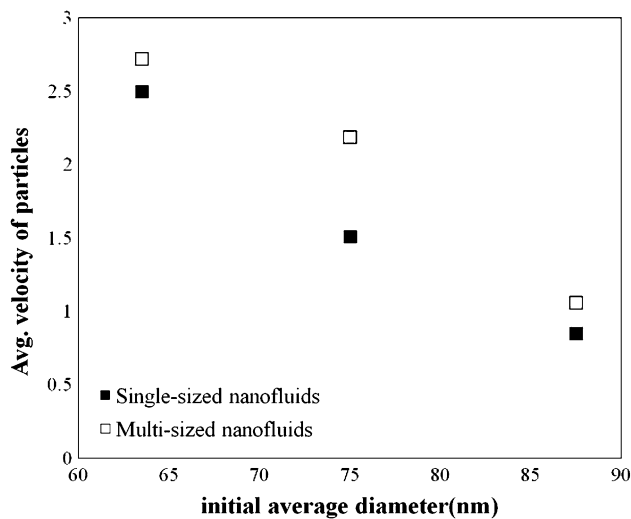
Fig. 7 The average velocity of particles for the multi-sized and corresponding single-sized nanofluids



Fig. 8 The average temperature two-way coupling values for the multi-sized and corresponding single-sized nanofluids

average particle velocity and average $q_{2w}$ of multi-sized cases from the corresponding single-sized case is larger for Cu(50 + 100 nm)/DIW nanofluids. The authors already showed in Fig. 3 that the heat transfer in fluid strongly depends on the velocity of the particles and the value of $\tau_T$. Thus, Figs. 7 and 8 indicate that both dispersion of particles and heat transport in nanoparticles contribute to the effect of multi-sized particles.

As shown above, it is clear that a greater enhancement of the energy transport inside the nanofluid was obtained when multi-sized particles were used. Both the average velocity of particles and average $q_{2w}$, which are critical for the enhancement of energy transport in nanofluids were observed to have greater magnitudes in the mixture cases. In order to understand the mechanism of particle velocity enhancement in mixture cases, the authors plotted the velocity of each individual particle in Fig. 9. The x-axis in the figure represents the particle number and the y-axis represents the velocity of each particles. Top graph of Fig. 9 shows the particle velocity for Cu(50 + 100 nm)/DIW and Cu(75 nm)/DIW nanofluids. To acquire a clear understanding of the plot, only a part of the data are shown in the figure. It is evident that the values of particle velocity in Cu(50 + 100 nm)/DIW nanofluid show greater fluctuations than the values in Cu(75 nm)/DIW nanofluids. The presence of multi-sized particles causes an inhomogeneous coagulations in the nanofluids, thus providing different ranges of velocity values in Cu(50 + 100 nm)/DIW nanofluid. But Cu(75 nm)/DIW nanofluid has smaller fluctuation magnitude in its profile. Since, the velocity of particles is strongly dependent on the diameter of the particles (shown in the Eqs. 6 and 8), the authors conclude that the coagulations of nanoparticles in Cu(75 nm)/DIW nanofluid are relatively more homogeneous than the
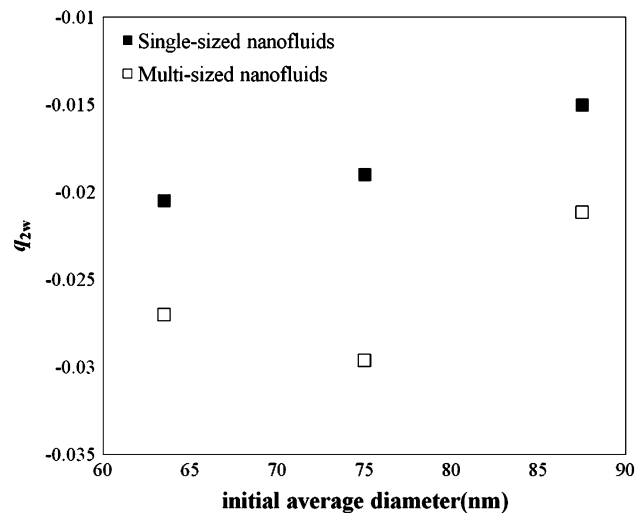
Cu(50 + 100 nm)/DIW multi-sized nanofluids. A similar observation can be made from lower graph of Fig. 9 where the particle velocities for Cu(75 + 100 nm)/DIW and Cu(87.5 nm)/DIW nanofluids are plotted. However, the fluctuations in the particle velocities in Cu(75 + 100 nm)/DIW nanofluid are not as dominant as in the Cu(50 + 100 nm)/DIW nanofluid. It can be concluded from the plot that the multi-sized nanofluids with larger initial particle size difference between them produce more inhomogeneous coagulations. These inhomogeneous coagulations lead to the distribution of wide range of particle sizes in multi-sized nanofluids. From Eq. 6, we can observe that the Brownian force $F_{Bi} \propto \sqrt{1/d_p^5}$. Thus smaller particles present in the multi-sized nanofluids have more dispersion which increases the average velocity of particles in comparison to single-sized nanofluids as found in Fig. 7. Figure 10, where $q_{2w}$ is plotted for different particles, reveals a similar consistent study. The fluctuations in $q_{2w}$ values for Cu(50 + 100 nm)/DIW nanofluid are larger than in the corresponding single-sized Cu(75 nm)/DIW nanofluid, indicating inhomogeneous coagulation of particles in multi-sized cases.

To measure the fluctuations, the standard deviations were calculated for both velocity of particles and $q_{2w}$. The values of average standard deviations are tabulated in Table 6. The comparison of multi-sized case with the corresponding single-sized case revealed greater average standard deviations for the multi-sized cases, thus indicating larger fluctuations in the velocity of particles and $q_{2w}$ for multi-sized cases. The average standard deviation values were found to be larger for the Cu(50 + 100 nm)/DIW nanofluid. It indicates that the inhomogenity in the coagulations increases with an increase in the size difference of initially distributed particles. In summary, in can be

**Fig. 9** Velocity of the particles is plotted for individual particles numbered from 3400–3450. Comparison for Cu(50 + 100 nm)/DIW and Cu(75 nm)/DIW nanofluids and Cu(75 + 100 nm)/DIW and Cu987.5)/DIW nanofluids is provided
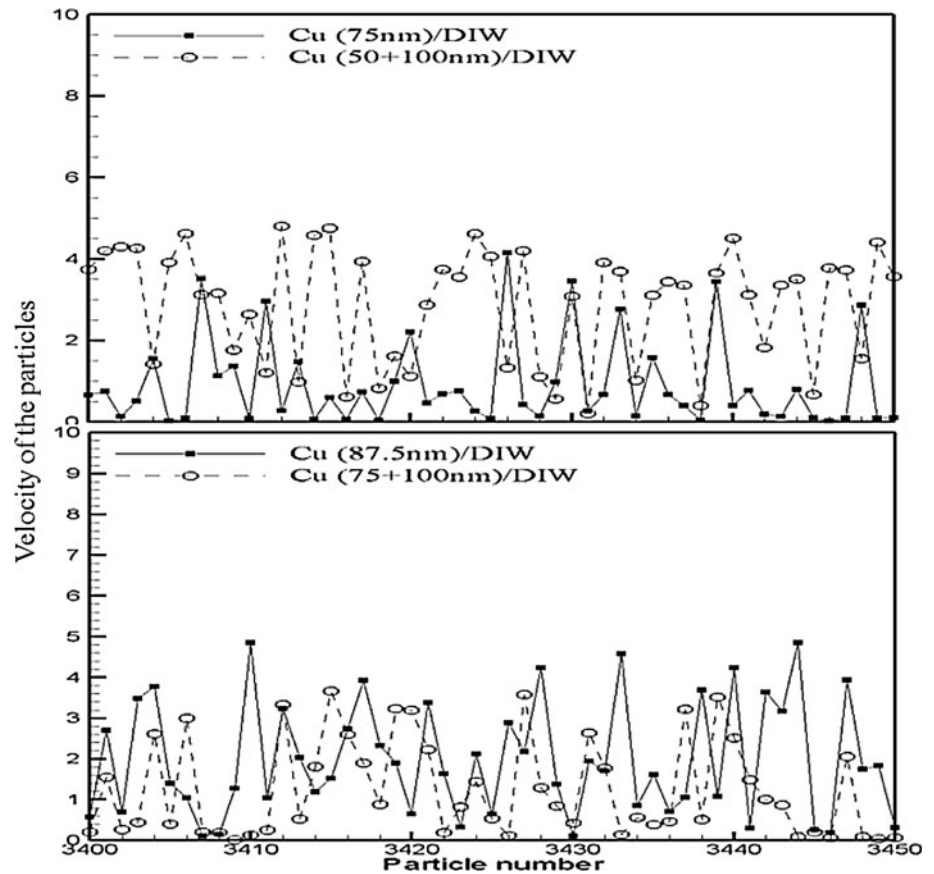


**Fig. 10** Temperature source term is plotted for individual particles numbered from 3400–450. Comparison for Cu(50 + 100 nm)/DIW and Cu(75 nm)/DIW nanofluids and Cu(75 + 100 nm)/DIW and Cu987.5)/DIW nanofluids is provided
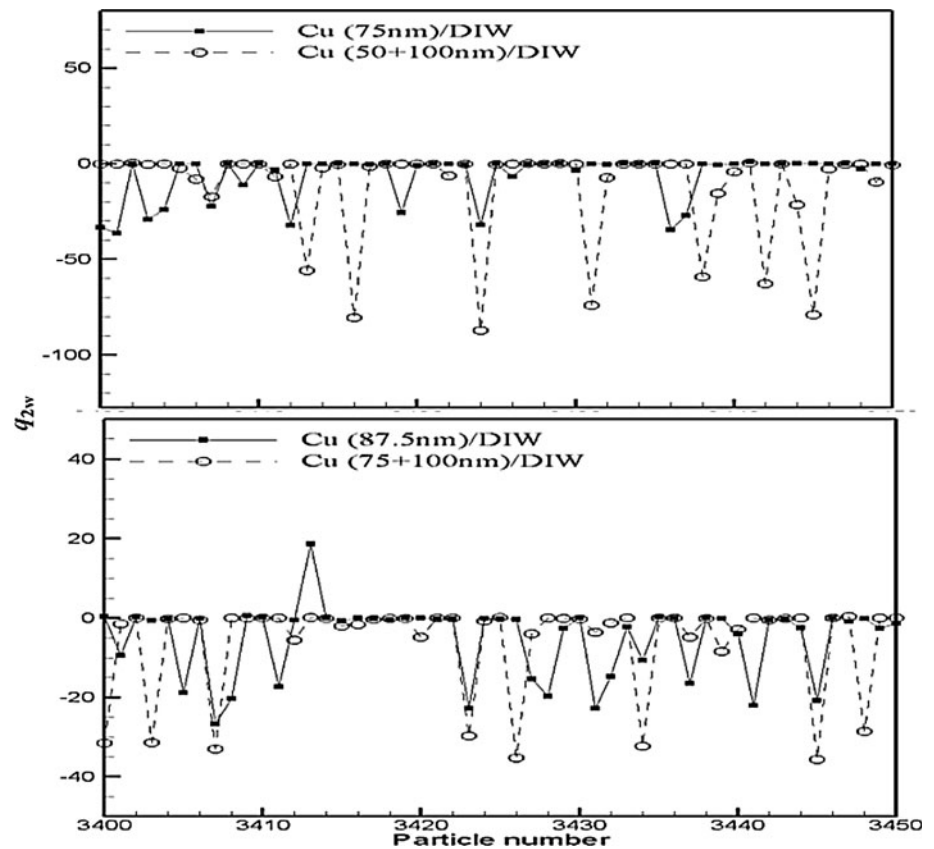
**Table 6** Average standard deviation values of the velocity of particles and temperature source term

| Nanofluid | Avg. standard deviation of velocity of particles | Avg. standard deviation of temperature source term |
|---|---|---|
| Cu(50 + 75 nm)/ DIW | 2.4837 | 16.1475 |
| Cu(63.5 nm)/DIW | 1.9489 | 12.5076 |
| Cu(50 + 100 nm)/ DIW | 1.7479 | 20.0803 |
| Cu(75 nm)/DIW | 1.2674 | 10.47 |
| Cu(75 + 100 nm)/ DIW | 1.3312 | 10.9934 |
| Cu(87.5 nm)/DIW | $9.301 \times 10^{-1}$ | 7.6743 |

said that the multi-sized particle distribution has a considerable effect on the effective thermal conductivity of nanofluids and thus all the numerical models when comparing with the experimental values should use an initial distribution similar to that of the experiments.

## 4 Conclusion

The effective thermal conductivity of nanofluids was found to alter significantly with the presence of multi-sized distribution of nanoparticles in fluid. The multi-sized nanofluid simulation predicted the effective thermal conductivity of nanofluid closer to the experimental value when compared to the volume weight averaged single-sized nanofluid.

The effect of multi-sized nanoparticle distribution on the heat transfer in nanofluids was studied by simulating nanofluids with multi-sized particles and corresponding single-sized particles. The study revealed that the dispersion of particles and the heat transport in nanoparticles were affected by the presence of multi-sized nanoparticles. Thus, both these mechanism had significant contributions in affecting the effective thermal conductivity of nanofluids.

Deviation in the effective thermal conductivity values was found to increase with the increase in the size difference in the initial distribution. It was also found that this deviation was more predominant when the particle sizes were smaller. The authors concluded that the inhomogeneous coagulations observed in the multi-sized particles can be responsible for the deviation of the effective thermal conductivity of multi-sized nanofluids from the single-sized nanofluids.

The authors, from this study conclude that initial distribution of particles has a significant role in predicting the effective thermal conductivity of nanofluids. The experimental data so far have been mostly reported using the volume averaged particle sizes. However, the authors suggest that the initial distribution of particles should be provided, while reporting the experimental results.

## References

Apostolou K, Hrymak AN (2008) Discrete element simulation of liquid-particle flows. Comput Chem Eng 32:841–856

Beck MP, Yuan Y, Warrier P, Teja AS (2009) The effect of particle size on the thermal conductivity of alumina nanofluids. J Nanopart Res 11:1129–1136

Canuto C, Hussaini MY, Quarteroni A, Zang TA (1987) Spectral methods in fluid mechanics. Springer, New York

Cardoso SSS, Zarrebini M (2001) Sedimentation of polydispersed particles from a turbulent plume. Chem Eng Sci 56:4725–4736

Choi SUS (1995) Enhancing thermal conductivity of fluids with nanoparticles. ASME FED 231:99–105

Choi SUS, Zhang ZG, Yu W, Lockwood FE, Grulke EA (2001) Anomalous thermal conductivity enhancement in nanotube suspensions. Appl Phys Lett 79:2252–2254

Chon CH, Kihm KD, Lee SP, Choi SUS (2005) Empirical correlation finding the role of temperature and particle size for nanofluid (Al$_2$O$_3$) thermal conductivity enhancement. Appl Phys Lett 87:153107

Ding Y, Wen D (2005) Particle migration in a flow of nanoparticle suspensions. Powder Technol 149:84–92

Eastman JA, Choi SUS, Li S, Thompson LJ (1997) Enhanced Thermal conductivity through the development of nanofluids. In: Proceedings of the symposium on nanophase and nanocomposite materials II, Materials Research Society, Boston, vol 457, pp 3–11

Eastman JA, Phillpot SR, Choi SUS, Keblinski P (2004) Thermal transport in nanofluids. Annu Rev Mater Res 34:219–246

Elperin T, Kleeorin N, Rogachevkii I (1996) Turbulent thermal diffusion of small inertial particles. Phys Rev Lett 76:224–227

Fujimoto T, Sy Terauchi, Umehara H, Kojima I, Henderson W (2001) Sonochemical preparation of single-dispersion metal nanoparticles from metal salts. Chem Mater 13:1057–1060

Keblinski P, Phillpot SR, Choi SUS, Eastman JA (2002) Mechanisms of heat flow in suspensions of nano-sized particles (nanofluids). Int J Heat Mass Transf 45:855–863

Kondaraju S, Jin EK and Lee JS (2009) Direct numerical simulation of thermal conductivity of nanofluids: the effect of temperature two-way coupling and coagulation of particles. Int J Heat Mass Transf. doi:10.1016/j.ijheatmasstransfer.2009.11.038

Li A, Ahmadi G (1992) Dispersion and deposition of spherical particles from sources in a turbulent channel flow. Aerosol Sci Technol 16:209–226

Li CH, Peterson GP (2006) Experimental investigation of temperature and volume fraction variations on the effective thermal conductivity of nanoparticle suspensions (nanofluids). J Appl Phys 99:084314

Maxey MR, Riley JJ (1983) Equation of motion for a small rigid sphere in a nonuniform flow. Phys Fluids 26:883–887

Mintsa HA, Roy G, Nguyen CT, Doucet D (2009) New temperature dependent thermal conductivity data for water-based nanofluids. Int J Therm Sci 48:363–371

Murshed SMS, Leong KC, Yang C (2006) A model for predicting the effective thermal conductivity of nanoparticles–fluid suspensions. Int J Nanosci 5:23–33

Murshed SMS, Leong KC, Yang C (2008a) Investigations of thermal conductivity and viscosity of nanofluids. Int J Thermal Sci 47:560–568

Murshed SMS, Leong KC, Yang C (2008b) Thermophysical and electrokinetic properties of nanofluids—a critical review. Appl Therm Eng 28:2109–2125

Spalart PR, Moser RD, Rogers MM (1991) Spectral methods for Navier-Stokes equations with one infinite and two periodic directions. J Comp Phys 96:297–324

Sundaram S, Collins LR (1999) A numerical study of the modulation of isotropic turbulence by suspended particles. J Fluid Mech 379:105–143

Talbot L, Cheng RK, Schefer RW, Willis DR (1980) Thermophoresis of particles in a heated boundary layer. J Fluid Mech 101:737–758

Timofeeva EV, Gavrilov AN, McCloskey JM, Tolmachev YV, Sprunt S, Lopatina LM, Selinger JV (2007) Thermal conductivity and particle agglomeration in alumina nanofluids: experiment and theory. Phys Rev E 76:061203

Wang X, Xu X, Choi SUS (1999) Thermal conductivity of nanoparticle–fluid mixture. J Thermophys Heat Transf 13:474–480

Wang X, Zhu D, Yang S (2009) Investigation of pH and SDBS on enhancement of thermal conductivity of nanofluids. Chem Phys Lett 470:107–111

Wen D, Ding Y (2005) Effect of particle migration on heat transfer in suspensions of nanoparticles flowing through minichannels. Microfluid Nanofluid 1:183–189

Xie HQ, Wang JC, Xi TG, Liu Y, Ai F, Wu QR (2002) Thermal conductivity enhancement of suspensions containing nanosized alumina particles. J Appl Phys 91:4568–4572

Xuan Y, Li Q (2000) Heat transfer enhancement of nanofluids. Int J Heat Fluid Flow 21:58–64

Xuan Y, Li Q, Hu W (2003) Aggregation structure and thermal conductivity of nanofluids. AIChE J 49:1038–1043

Zhu H, Zhang C, Liu S, Tang Y, Yin Y (2006) Effects of nanoparticles clustering and alignment on thermal conductivities of $Fe_3O_4$ aqueous nanofluids. Appl Phys Lett 89:023123

Zhu D, Li X, Wang N, Wang X, Gao J, Li H (2009) Dispersion behavior and thermal conductivity characteristics of $Al_2O_3$–$H_2O$ nanofluids. Curr Appl Phys 9:131–139